THE ASTROPHYSICAL JOURNAL, 355:645–650, 1990 June 1

OBSERVATION OF THE CRAB PULSAR, PSR 0531+21, AT 0.2–6.0 MeV WITH THE FIGARO II EXPERIMENT

B. AGRINIER,[1] J. L. MASNOU,[2] B. PARLIER,[1] M. NIEL,[3] P. MANDROU,[3] G. VEDRENNE,[3] G. GERARDI,[4] T. MINEO,[5] B. SACCO,[5] L. SCARSI,[4,5] E. COSTA,[6] E. MASSARO,[7] G. MATT,[7] M. SALVATI,[8] AND A. G. LYNE[9]

Received 1989 June 29; accepted 1989 November 15

ABSTRACT

Observations of the Crab pulsar (PSR 0531+21) in the energy range 0.2–6 MeV have been made with the balloon-borne FIGARO II experiment. The gross appearance of the light curve is characterized by the well-known double-peak structure with a phase separation of 0.4. Our data confirm that the second pulse is the dominant feature, and the interpulse region is more luminous than in other energy ranges. Above $\sim$0.5 MeV, we can detect in the light curve an extra structure, with two features at a phase lag of 0.4 as the main one. Phase-resolved spectroscopy indicates that the first peak spectrum is concave upward, and the second one is concave downward, while the averaged spectrum is well represented by a single power law with slope 2.2.

The good timing accuracy of FIGARO allowed us to measure a delay between gamma rays and radio waves of 300 ± 70 μs, that if produced by dispersion, implies a value of DM fitting very well the radio measurements 2 months before and after our observation.

Subject headings: gamma rays: general — nebula: Crab Nebula — pulsars — stars: individual (PSR 0531+21) — stars: radio radiation

I. INTRODUCTION

A strategically important energy range for the observation of pulsars is in the soft γ-rays (between 0.1 and 10 MeV typically). On the other hand, theory predicts that the primary output of a pulsar is in the hard (or even very hard) γ-rays; on the other hand, the observations are almost exclusively concentrated in the radio domain, which is believed to be the by-product of a chain of downgrading processes. The transition from the primary to the secondary radiation mechanisms should occur precisely at low γ-ray energies.

Evidence for this to be the case is provided by the two most active pulsars, PSR 0531+21 and PSR 0833−45, which have very similar properties in the hard γ-ray range, but differ drastically at all lower frequencies, including the X-rays and the optical (see, for instance, Bignami and Hermsen 1983). While the more robust primary mechanism is less sensitive to the pulsar parameters, the secondary mechanisms depend on the interaction of several factors and vary strongly with relatively modest differences such as a factor of 3 in period, as for the two above-mentioned objects. By the same token, the transition region should contain information on details of the magnetospheric structure and particle flows around the pulsar (e.g., Salvati 1983; Cheng, Ho, and Ruderman 1986*a*, *b*).

In order to explore the soft γ-ray emission from pulsars, we made use of the FIGARO experiment, an acronym for French Italian GAmma Ray Observatory. FIGARO is a large area, actively shielded, noncollimated detector for photons in the energy range 0.17–6.0 MeV, to be operated at high altitude by means of a stratospheric ballon; it is specifically designed to observe cosmic sources with a well-established time signature. Uncollimated experiments were already used successfully to study the γ-ray emission from the Crab pulsar, e.g., by Kurfess (1971), and Wilson and Fishman (1983). A first version of FIGARO was completed in 1982 (Agnetta *et al.* 1983) and was heavily damaged by a free-fall following a balloon burst in 1983. A second improved version, called FIGARO II, was successfully flown in the northern sky in 1986.

In the following we present a detailed account of our data on PSR 0531+21. More precisely § II is a brief description of the experiment, and of the flight conditions Section III deals with the techniques we used for temporal and spectral analysis. Section IV contains the final results, and a discussion of the spectral behavior of the "canonical" components of the light curve; we also attempt a noncanonical approach with correlation functions in order to bring up more clearly possible "new" components. Finally, we give our conclusion in § V.

II. EXPERIMENT AND FLIGHT PARAMETERS

The principal detector of FIGARO II is a square array of nine NaI(Tl) tiles with a total geometric area of 3600 cm^2 and a thickness of 5 cm. The principal detector is actively shielded against the environmental background by a wall of 12 NaI(Tl) modules along the four sides, and by four blocks of plastic scintillators from below. Another plastic scintillator (5 mm thick) is placed on the top of the whole experiment to anticoincide charged particles. In order to reduce the background at high energy, each module of the principal detector was set in anticoincidence with the neighboring ones. Gain variations of the nine photomultipliers (PMT's) of the principal detector are monitored by means of a tagged, low-activity ^{22}Na source located well above the top shield. Signals from the modules of the main detector, when no veto from the various anticoincidences is present, are transmitted one by one via an asynchronous telemetry channel with 300 kHz bandwidth.

Considering the complex geometry of the experimental and

[1] Service d'Astrophysique, DPhG, CEN, Saclay.
[2] UPR176, DARC, Observatoire de Paris, Section de Meudon.
[3] CESR, Université P. Sabatier, Toulouse.
[4] Universitá di Palermo and Unitá GIFCO, CNR, Palermo.
[5] Istituto di Fisica Cosmica e Applicazioni all' Informatica, CNR, Palermo.
[6] Istituto di Astrofisica Spaziale, CNR, Frascati.
[7] Istituto Astronomico, Universitá "La Sapienza," Roma.
[8] Osservatorio Astrofisico di Arcetri, Firenze.
[9] University of Manchester, Nuffield Radio Astronomy Laboratories, Jodrell Bank.

the anticoincidence logic, the evaluation of the instrumental response was not left to numerical simulation alone. The experiment was calibrated by using a set of radioactive sources at different inclinations to the axis. Spectra from different calibrators were fitted with semiempirical functional forms, describing to a good accuracy even the details of measured features. After smoothing and interpolating in energy, the matrix of response with energy and direction was obtained. A complete description of FIGARO II, including a discussion of the calibrations and the in-flight performances, can be found in Agnetta *et al.* (1989).

The experiment was launched from the Milo base (Trapani, Italy; latitude 38°00′ N, longitude 12°35′ E) on 1986 July 11 at 5 hr U.T. (JD 2,446,622.7) with a hydrogen-inflated balloon of 830,000 cubic meters. A float altitude corresponding to 4.0 mbar residual pressure was reached 3 hr later and was kept with practically no variations for the entire flight. The average measured counting rate was 1360 counts s^{-1}, in agreement with the results of Monte Carlo simulations.

Transmitted data were accumulated on ground by means of an analogic tape recorder. At the Milo base, a UTC generator driven by a rubidium clock allowed a relative timing with a precision of 10 μs; absolute timing was obtained by trasportation of a second atomic clock from the Time Service of the Istituto Galileo Ferraris (Turin), and subsequent control via television synchronism; the effective overall precision on the photon arrival times includes the numerization of the analogic tape and is better than 30 μs under standard conditions.

During the final part of the ascent and for 2.5 hr at ceiling, the experiment was pointed in the direction of the Crab pulsar; at $10^{h}25^{m}$ U.T. the Crab observation was terminated due to a temporary failure of the telemetry.

III. DATA ANALYSIS

The light curves and spectra of the Crab pulsar presented here have been obtained by means of the folding technique. The arrival times of the accepted photons were converted to the solar system barycenter using the MIT ephemerides PEP311 (Ash, Shapiro, and Smith 1967). The ephemerides of the pulsar itself at observation epoch have been derived from a nearly contemporary radio measurement (1986 July 15; Lyne, Pritchard, and Smith 1988). The adopted values of the frequency and frequency derivatives were $\nu_0 = 30.0063102177$ Hz and $\nu_0' = -379318.56 \times 10^{-15}$ s^{-2} at the reference time $t_0 =$ 2,446,626.5. The phases $\phi(t)$ of the single photons have been calculated according to the relation

$$\phi(t) = \nu_0(t - t_0) + \nu_0' \frac{(t - t_0)^2}{2}$$

and then used to derive phase histograms. The content of each phase bin has been corrected for the dead time. Figure 1 shows the pulse profile for the energy range 0.2–6.0 MeV with a phase resolution of 60 bins.

The well-known double-peaked signal of PSR 0531+21 is clearly apparent, with the pulses separated by 0.40, and a significant emission in the interpulse region. In the following, we take phase zero at the center of the first peak.

In uncollimated experiments like the present one, the choice of the off-pulse phase range to be used as background is obviously crucial. Here we have taken an (initially narrow) interval around phase 0.65, best fitted the observed counts to a constant, and studied the behavor of the χ^2 while the interval was

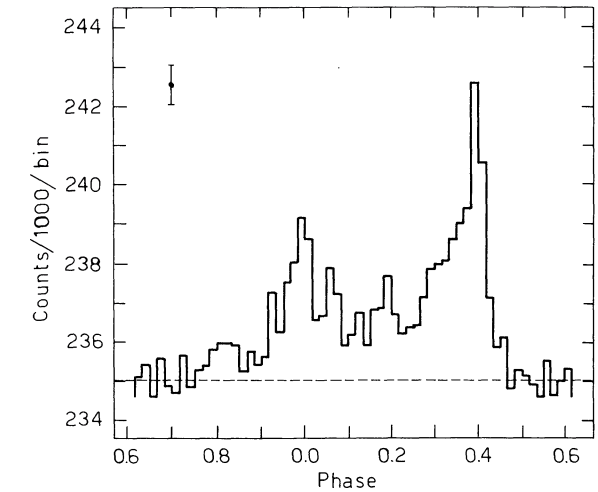

FIG. 1.—Phase histogram of PSR 0531+21 for $0.2 < E_{ph} < 6.0$ MeV

extended progressively on both sides. The largest possible phase range with $\chi^2_{dof} < 1$ is 0.47–0.77. The transfer matrix through the residual atmosphere has been computed up to the first Compton scattering. With the instrument pointing to the zenith under d g cm^{-2} of air, we considered a vertical beam of photons of a given initial energy; the matrix includes the photons propagating directly through d, plus those which have a Compton scattering before d, and then survive the remaining travel to the experiment; for the scattered photons, the shadow of the lateral shielding was included. The relevant cross-sections, Compton and total, were computed according to Massaro, Costa, and Salvati (1982). The variable value of d during ascent, and the variable value of the effective d during tracking are taken into account; when the instrument is pointing off the zenith, the effects of a nonparallel atmosphere are neglected.

IV. RESULTS AND DISCUSSION

a) Structure of the Pulse Profile

Ideally, pulsar data should be described as a surface in a three-dimensional space representing energy, phase, and photon number; we give instead projections on the two coordinate planes separately. Figure 1 is the light curve in the whole FIGARO bandwidth; the gross appearance is similar to what was already known in the adjacent spectral regions, in particular the two peaks at 0.40 phase separation with sharper edges on the outside, and a rounder " valley " in the interpulse region. There are, however, important peculiarities. The most obvious one is the dominance of the second peak, which in the X-rays and in the hard γ-rays is only a fraction of the first one (an effect already noted in previous observations, see White *et al.* 1985 for a summary of the data); also apparent is the high level of the interpulse emission, similar to the hard X-rays (Hasinger *et al.* 1984), and higher than other energy ranges. A new interesting result is that the light curve has additional structure besides the main peaks: especially evident are the extra features at phases around 0.2 and 0.8.

In Figure 2, panels *a*, *b*, and *c*, we present the light curve of PSR 0531+21 in three different energy ranges within our total bandwidth, with a phase resolution which decreases progressively in order to compensate for the decreasing counts. At the highest energies, panel *c*, only the main structure is visible; but the comparison between panels *a* and *b* indicates a different

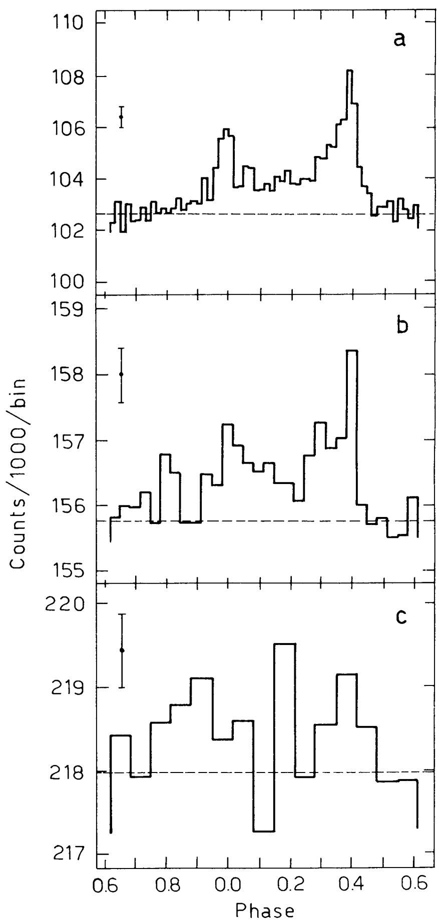

FIG. 2.—Phase histograms of PSR 0531+21 for $0.2 < E_{ph} < 0.45$ MeV (*a*), $0.45 < E_{ph} < 1.3$ MeV (*b*), and $1.3 < E_{ph} < 6.0$ MeV (*c*).

spectral behavior of different portions of the light curve; note, for instance, the hardness of the region around phase 0.8 as compared with the first main peak at phase 0.0. Such a complex pattern is better discussed in terms of phase-resolved spectroscopy, which we tackle in the following subsection.

b) *Phase-resolved Spectroscopy*

Figure 3 is the deconvolved spectrum averaged over the nonbackground phase interval, 0.77–0.47. The data can be fitted with a power law with amplitude $6.93 \pm 0.26 \times 10^{-4}$ photons cm^{-2} s^{-1} MeV, and exponent 2.25 ± 0.58, which is also shown in the figure. Both the normalization and the slope appear to be in good agreement with previous measurements

TABLE 1

BEST FIT PARAMETERS FOR THE SPECTRA OF FIVE DIFFERENT PHASE INTERVALS[a]

Interval	Phase	A (photons cm^{-2} s^{-1} MeV^{-1})	α
1...........	0.77–0.95	$(1.29 \pm 0.43)10^{-4}$	1.20 ± 0.37
2...........	0.95–0.05	$(1.49 \pm 0.05)10^{-4}$	2.14 ± 0.07
3...........	0.05–0.19	$(8.60 \pm 0.50)10^{-5}$	2.50 ± 0.10
4...........	0.19–0.33	$(1.64 \pm 0.04)10^{-4}$	2.22 ± 0.07
5...........	0.33–0.47	$(2.71 \pm 0.13)10^{-4}$	2.13 ± 0.06

[a] According to the law $dN/dE = A(E/1 \text{ MeV})^{-\alpha}$.

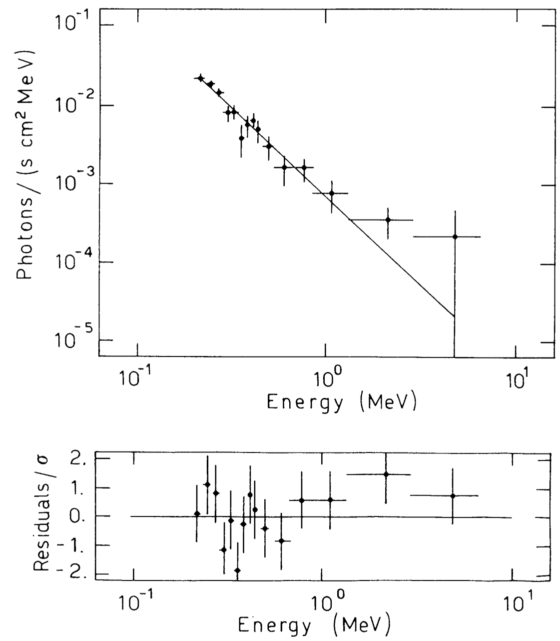

FIG. 3.—Deconvolved spectrum and best power-law fit to the pulsed signal in the phase interval 0.77–0.47; the lower panel shows the residuals in terms of the relevant standard deviation.

in adjacent and/or overlapping energy ranges (see the compilation of Knight 1983; Mahoney, Ling, and Jacobson 1984; White *et al.* 1985); however, after a more detailed analysis the apparent uniformity is found to result from the compensation of several diverging trends.

Because of the good statistics provided by FIGARO, we can divide our data into five phase intervals and still derive a meaningful power-law fit to the spectrum of each of them; Table 1 lists the interval boundaries and the best fitting amplitudes and slopes.

The slope as a function of phase is plotted in Figure 4 (note that intervals number 2 and 5 fall on the first and second peak, respectively): our analysis confirms the suggestion of Figure 2 that the phase region just before the first peak is very hard. The spectrum softens gradually and regularly with increasing phase, up to and including the rightmost portion of the inter-

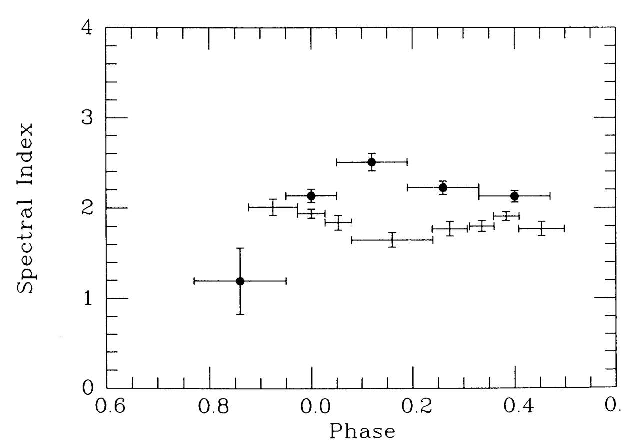

FIG. 4.—Phase-dependence of the spectral index of the best power-law fit of our data (0.2–6 MeV; *filled circles*) compared with that found by Knight (1982) at lower energies (18–200 keV).

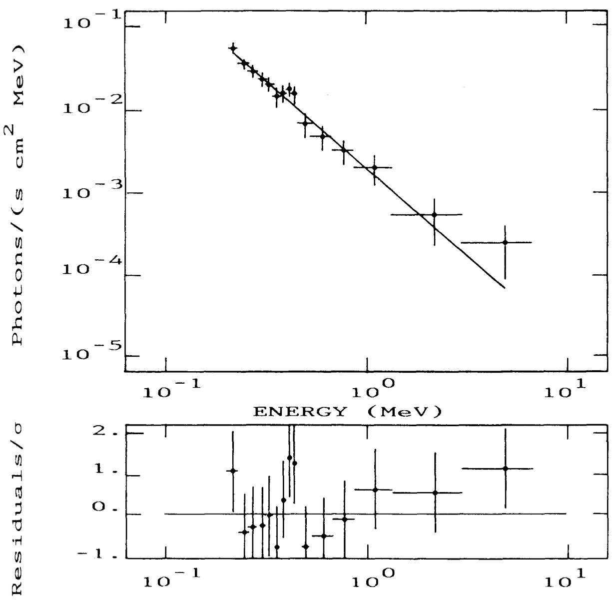

FIG. 5.—Same as Fig. 3, for the phase interval corresponding to the second peak (0.27–0.47); note the excess residual at $E_{ph} \sim 0.4$ MeV.

pulse; the second peak is harder again, more or less at the level of the first one. In the same figure we give the corresponding quantities for the energy interval 18–200 keV (Knight 1982): the different behavior of the interpulse region is well evident. Hasinger *et al.* (1984) fit the interpulse data from ~50 keV to ~1 GeV with a power law of 2.24. This is fully compatible with our findings in phase interval no. 4 (0.19–0.33), but a more detailed comparison is impossible, since Hasinger *et al.* (1984) do not give the phase boundaries of their adopted interpulse.

Figure 5 gives the best power-law fit in the phase interval corresponding to the second peak; the excess in the residuals at ~0.4 MeV, although statistically not compelling (1.8 standard deviations), is reminiscent of a similar feature reported by Leventhal, MacCallum, and Watts (1977) and Ayre *et al.* (1983) for the total flux (1.3., pulsar plus nebula).

Further information can be gained from phase-resolved spectroscopy in a range of energies wider than, and including, the FIGARO bandwidth. In order to do so, we restricted only to three phase intervals, namely 0.95–0.05 (first pulse), 0.05–0.33 (interpulse), and 0.33–0.47 (second pulse) and computed, from several published light curves (from optical to gamma rays), the ratios of second to first pulse (P2/P1), interpulse to first pulse (Int/P1), and interpulse to second pulse (Int/P2), after subtraction of the off-pulse background, evaluated in the same phase interval as our data.

The results are displayed in Figure 6, panels *a*, *b*, and *c*. Precisely at FIGARO energies, the first peak reaches a minimum relative to both the second one and the interpulse region; always at FIGARO energies, the interpulse reaches a maximum relative not only to the first peak, but also to the second one. Since the phase-averaged spectrum of the Crab pulsar is well represented by a single power law with slope 2.2, one concludes that the first pulse spectrum is concave upward, while the second one is concave downward, the flexion points occurring somewhere in the soft γ-rays. One further concludes that the interpulse spectrum also is concave downward, with a larger curvature than the second pulse, and a lower value for the break energy, as implied by Figure 4.

Our approach is meaningful only if the pulse profile is time-steady. Above 50 MeV, from the *COS B* observations spanning 7 yr (Clear *et al.* 1987) we know that the ratio P2/P1 varied by a factor of about 3; at lower energies (50 keV–0.3 MeV) Mahoney, Ling, and Jacobson (1984) do not find any change of the pulse shape from fall 1979 to spring 1980. In the low-energy γ-rays no firm evidence for or against stability has been provided so far, and this point is certainly worthy of a better understanding.

c) Secondary Structure

Next we comment about the significance of the "extra" structure appearing in the light curve. We are not the first ones to note additional peaks: Kurfess (1971), working in the energy range 100–400 keV, explicitly points out the presence of a feature at phase 0.8. Furthermore, in Figure 1 there is a hint of

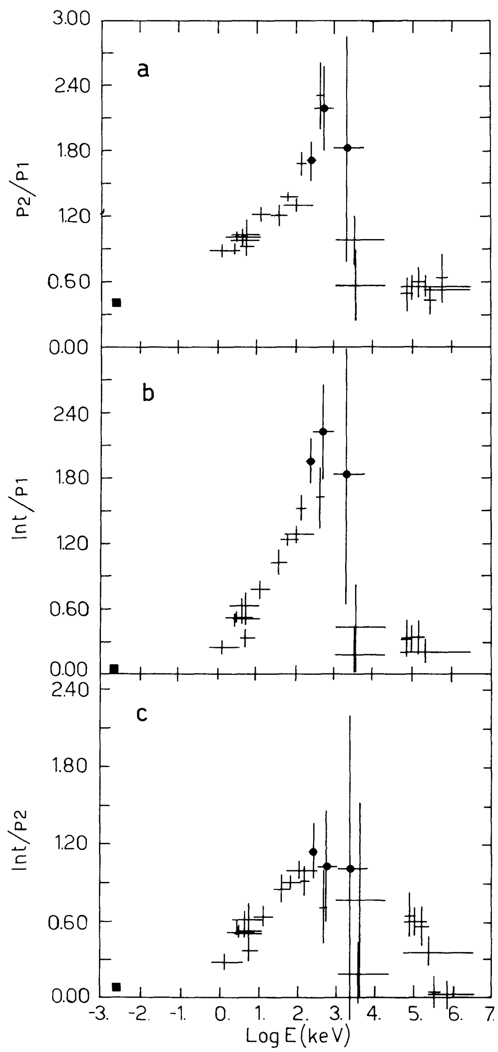

FIG. 6.—Ratio of second peak to first peak (*a*), interpulse to first peak (*b*), and interpulse to second peak (*c*), from a compilation of literature data; see text for the phase interval boundaries. References: Optical/UV (*squares*): Cocke and Ferguson (1974); X-rays: Kestenbaum *et al.* (1976); Kanbach *et al.* (1977); Weisskopf *et al.* (1978); Wills *et al.* (1982); Harnden and Seward (1984); hard X-rays: Hameury *et al.* (1983); Wilson and Fishman (1983); Mahoney, Ling, and Jacobson (1984); γ-rays: Graser and Schonfelder (1982); White *et al.* (1985); Clear *et al.* (1987). The filled circles are FIGARO data.

excess photons in the bins around phase 0.2: This is important, since the excess would lag the above extra by 0.4, and 0.4 is the phase difference between the main pulses at all frequencies in PSR 0531 + 21, and at hard γ-ray frequencies in PSR 0833 − 45. It is conceivable that such a "universal" phase difference is related to some basic geometrical fact, as the location and orientation of an outer gap (Cheng, Ho, and Ruderman 1986*b*); then the appearance in our energy window of a second, weaker pair of pulses with just that phase difference would be the signal of yet another gap entering the line of sight. Note also that a phase difference of 0.2 is of the order of the light travel time over a light cylinder radius.

In order to put on a more quantitative footing the above considerations, we have convolved the observed light curve with a "skeleton" light curve: the latter has two triangular peaks of height 1 and width 0.05 separated by 0.4 and is 0 everywhere else. Before convolution, the observed curve is normalized to 1, and the mean value is subtracted. The results are shown in Figure 7 for photon energies below (panel *a*) and above (panel *b*) $E_{ph} = 0.42$ MeV: the three largest maxima correspond to the filter covering both or either one of the main pulses; in panel *b*, however, there is a quite significant fourth maximum, which is due to the secondary pulse pair under discussion.

We have convolved the same filter with a control light curve, generated at random with the same binning and the same average count rate of the real one; we did not get a signal as strong as the one in Figure 7 in any of the 10^4 trials performed.

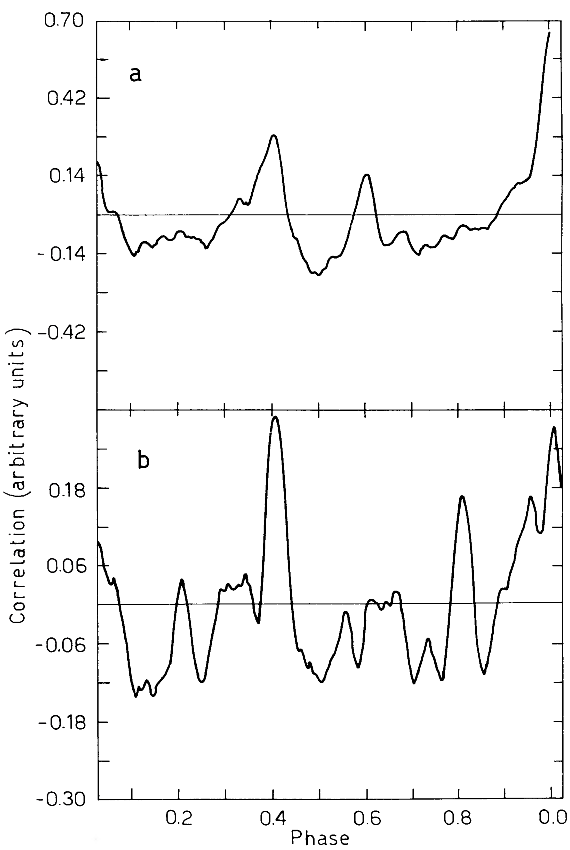

FIG. 7.—Cross-correlation function for $E_{ph} < 0.42$ MeV (*a*), and $E_{ph} > 0.42$ MeV (*b*); see text for definitions and normalizations; our signal is the peak at phase 0.8 in (*b*).

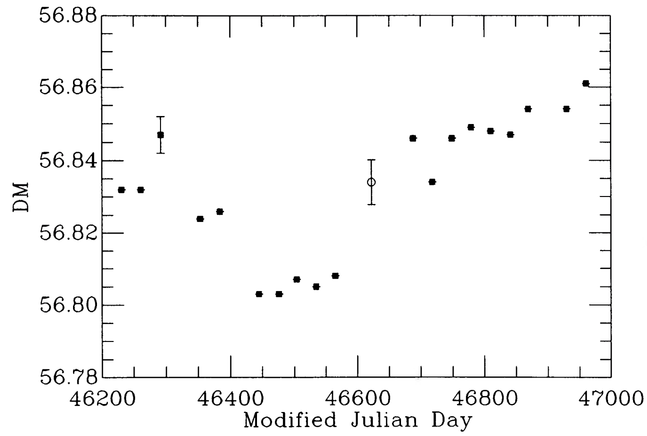

FIG. 8.—Dispersion measure DM plotted as a function of the current date; the squares are radio-only data (a typical error bar is also shown), the circle point is from FIGARO.

d) *Absolute Timing*

Previous γ-ray experiments have demonstrated the simultaneity of the radio and γ-ray main peaks within 1 ms. The good timing accuracy of FIGARO allows a more precise measurement of a possible time difference, down to 0.1 ms.

The ephemerides adopted for the γ-ray analysis are the same ones which were used by Lyne, Pritchard, and Smith (1988) in order to obtain the radio pulses's arrival times. The effects of dispersion are corrected for by observing at two different radio frequencies; the dispersion measure DM in the Jodrell Bank Monthly Ephemeris is provided with a typical error of 0.005 pc cm^{-3}. The observations were made mostly at a frequency of 610 MHz and the time at infinite frequency follows from

$$t_{\infty} = t_{610\,\mathrm{MHz}} - 0.0112\ \mathrm{DM}\ s\ .$$

The value of DM was not measured at Jodrell Bank between 1986 May 15 (when DM = 56.808 pc cm^{-3}) and 1986 September 15 (when DM = 56.846 pc cm^{-3}); these values differ by much more than the quoted error and imply a variation in $t_{610\,\mathrm{MHz}} > 400$ μs. In the intervening period, the t_{∞} tabulated by Lyne, Pritchard, and Smith (1988) was computed assuming the value of DM measured on 1986 May 15.

In order to evaluate the best position of the main γ-ray peaks, we have fitted the observed light curve with a set of Gaussians plus a constant level in the relevant phase intervals. On the one hand, we find a phase delay between the main peaks equal to 0.403 ± 0.003, in perfect agreement with the Jodrell Bank result 0.40402 ± 0.00001. On the other hand, we obtain a γ-ray arrival preceding the *published* radio time by 300 ± 70 μs. The discrepancy disappears if one adopts a value of DM = 56.834 pc cm^{-3}, intermediate between the quoted radio values; in other words, here we have a direct measure of DM, where t_{∞} is not deduced by extrapolation but provided by t_{γ}. Figure 8 is a plot of DM in function of time with the FIGARO point added to the radio data.

V. CONCLUSIONS

We have reported on the analysis of the data on the Crab pulsar collected with the FIGARO experiment during the transmediterranean flight of 1986 July 11. Our data give additional information in an energy band which is expected to provide very important diagnostics for a theory of the pulsar magnetosphere. We have found evidence for complex spectral

1990ApJ...355..645A

behavior of the various components of the light curve; in particular the sharp decrease of the ratio between the interpulse and the second pulse to the first one above ~ 0.5 MeV hints at some phenomenon in the emission mechanisms linked to the electron rest mass.

The detection, in the same range, of an extra structure with two features at the same phase lag as the main one could have interesting implications on the geometry of the emission. We know with sufficient certainty that the pulsar magnetosphere is dominated particle-wise by negatrons and positrons; however, the rest mass signature could be visible from a cold, as opposed to relativistic, electron plasma. This could be accommodated only in selected locations, different from the "gaps" where the higher energy γ-rays are produced, adding further complication to the models.

Finally, we have confirmed the coincidence between radio and γ-ray peaks; in fact, due to the good timing accuracy of our experiment, we have measured DM at a time when only single-frequency radio observations were available.

More extended observation would allow a better assessment of the observed features and provide information on their stability in time. A further point of relevance here is the possible relation between variability and the occurrence of period glitches, as suggested by recent data on the Vela pulsar (Sacco *et al.* 1990): the Crab pulsar, in fact, has just undergone the largest glitch ever observed (Lyne and Pritchard 1989).

The comparision between light curves obtained with the same instrument at different epochs is a most direct approach to the variability issue. FIGARO II is scheduled for a second transmediterranean flight in 1990, and the Crab pulsar will be the main target of the campaign.

We are greatly indebted to I. Shapiro for providing PEP311 on tape, and to D. Richards for the barycentering software. We also acknowledge the financial support of CNES and the Piano Spaziale Nazionale, and the help of the many persons from CESR, CNES, CEN Saclay, and CNR who have contributed to the preparation of the FIGARO payload and to the flight campaigns; among them, we would like to mention explicitly A. Soubrier, strong-handed leader of the launching team. The drawings were prepared by A. Lepre.

REFERENCES

Agnetta, G., *et al.* 1983, *Adv Space Phys.*, **3**, 113.
Agnetta, G., *et al.* 1989, *Nucl. Instr. Methods A*, **281**, 197.
Ash, M. E., Shapiro, I. I., and Smith, W. B. 1967, *A.J.*, **72**, 338.
Ayre, C. A., Bhat, P. N., Ma, Y. Q., Myres, R. M., and Thompson, M. G. 1983, *M.N.R.A.S.*, **205**, 285.
Bignami, G. F., and Hermsen, W. 1983, *Ann. Rev. Astr. Ap.*, **21**, 67.
Cheng, K. S., Ho, C., and Ruderman, M. 1986*a*, *Ap. J.*, **300**, 500.
———. 1986*b*, *Ap. J.*, **300**, 522.
Clear, J., *et al.* 1987, *Astr. Ap.*, **174**, 85.
Cocke, W. J., and Ferguson, D. C. 1974, *Ap. J.*, **194**, 725.
Graser, U., and Schonfelder, V. 1982, *Ap. J.*, **263**, 677.
Hameury, J. M., *et al.* 1983, *Ap. J.*, **270**, 144.
Harnden, F. R., and Seward, F. D. 1984, *Ap. J.*, **283**, 279.
Hasinger, G., Pietsch, W., Reppin, C., Trumper, J., Voges, W., Kendziorra, P., and Staubert, R. 1984, *Adv. Space Res.*, **3**, 63.
Kanbach, G., *et al.* 1977, *Proc. 12th ESLAB Symp.* (ESA-SP 124), p. 21.
Kestenbaum, H. L., Novick, R., and Wolff, R. S. 1976, *Ap. J.* (*Letters*), **203**, L57.
Knight, F. K. 1982, *Ap. J.*, **260**, 538.
———. 1983, in *Positron-Electron Pairs in Astrophysics*, ed. M. L. Burns, A. K. Harding, and R. Ramaty (New York: AIP), p. 141.
Kurfess, J. D. 1971, *Ap. J.* (*Letters*), **168**, L39.
Leventhal, M., MacCallum, C. J., and Watts, A. C. 1977, *Nature*, **266**, 696.
Lyne, A. G., and Pritchard, R. S. 1989 *IAU Circ.* No. 4845.
Lyne, A. G., Pitchard, R. S., and Smith, F. G. 1988, *M.N.R.A.S.*, **233**, 667.
Mahoney, W. A., Ling, J. C., and Jacobson, A. S. 1984, *Ap. J.*, **278**, 784.
Massaro, E., Costa, E., and Salvati, M. 1982, *Nucl. Instr. Methods*, **192**, 423.
Sacco, B., *et al.* 1990, *Ap. J.* (*Letters*), **349**, L21.
Salvati, M. 1983, *Space Sci. Rev.*, **36**, 145.
Weisskopf, M. C., Silver, E. H., Kestenbaum, H. L., Long, K. S., and Novick, R. 1978, *Ap. J.* (*Letters*), **220**, L117.
White, R. S., Sweeney, W., Tumer, T., and Zych, A. 1985, *Ap. J.* (*Letters*), **299**, L23.
Wills, R. D., *et al.* 1982, *Nature*, **296**, 723.
Wilson, R. B., and Fishman, G. J. 1983, *Ap. J.*, **269**, 273.

B. AGRINIER and B. PARLIER: CEN-Saclay, DPhG/SAP, 91191 Gif-sur-Yvette CEDEX, France

E. COSTA: Istituto di Astrofisica Spaziale, CNR, via E. Fermi 21, 00044 Frascati, Italy

G. GERARDI: Istituto di Fisica, Università di Palermo, Via Archirafi 36, 90136 Palermo, Italy

A. G. LYNE: University of Manchester, Nuffield Radio Astronomy Laboratories, Jodrell Bank, Macclesfield, Cheshire SK11 9DL

P. MANDROU, M. NIEL, and G. VEDRENNE: Centre d'Etude Spatiale des Rayonnements (CNRS-UPS), B.P. 4346, 31029 Toulouse CEDEX, France

J. L. MASNOU: DARC, UPR 176, Observatoire de Paris, Section de Meudon, 5, Place J. Janssen, 92195 Meudon, France

E. MASSARO and G. MATT: Istituto Astronomico dell'Università di Roma "La Sapienza," via G. M. Lancisi 29, 00161 Roma, Italy

T. MINEO, B. SACCO, and L. SCARSI: Istituto di Fisica Cosmica e Applicazioni all'Informatica, CNR, via M. Stabile 172, 90139 Palermo, Italy

M. SALVATI: Osservatorio Astrofisico di Arcetri, Largo E. Fermi 5, 50125 Firenze, Italy